JOHNSON MATTHEY
TECHNOLOGY REVIEW
www.technology.matthey.com

Johnson Matthey Highlights

A selection of recent publications by Johnson Matthey R&D staff and collaborators

NON-PEER REVIEWED FEATURE

Received 17th March 2022; Online 6th April 2022

Operando XAFS Investigation on the Effect of Ash Deposition on Three-Way Catalyst Used in Gasoline Particulate Filters and the Effect of the Manufacturing Process on the Catalytic Activity

M. Panchal, J. Callison, V. Skukauskas, D. Gianolio, G. Cibin, A. P. E. York, M. E. Schuster, T. I. Hyde, P. Collier, C. R. A. Catlow and E. K. Gibson, *J. Phys.: Condens. Matter*, 2021, **33**, (28), 284001

Operando XAFS was performed on two model GPF systems, one from a catalyst washcoat not previously adhered to a GPF and the other which contained ash components extracted from a GPF (20 g ash). The catalytic activity profiles of the systems were compared to a GPF containing no ash components (0 g ash). The 20 g ash sample had a higher carbon monoxide light off temperature than the 0 g ash sample. It also demonstrated an oscillation profile for carbon monoxide, carbon dioxide and oxygen. Post ageing, the washcoat and 0 g ash samples reduced NO at 310ºC, whereas the 20 g sample maintained a higher temperature. The presence of ash combined with high temperature ageing was thought to have an irreversible negative impact on catalyst performance.

Restructuring Effects in the Platinum-Catalysed Enantioselective Hydrogenation of Ethyl Pyruvate

G. A. Attard, A. M. S. Alabdulrahman, D. J. Jenkins, P. Johnston, K. G. Griffin and P. B. Wells, *Top. Catal.*, 2021, **64**, 945

Three series of 5% platinum/graphite catalysts were prepared. One was sintered in pure argon, while the other two series were sintered in 5% hydrogen/argon. {100}-terraces, {111}-terraces and stepped features were observed on the platinum surfaces by CV. The catalytic performance of the surface structures in the enantioselective hydrogenation of ethyl pyruvate to ethyl lactate was revealed. Progressive platinum particle growth with surface restructuring and faceting was observed for the two catalysts sintered in 5% hydrogen/argon. Of these two series, the one containing smaller platinum particles encompassed a higher fraction of surface Pt{111}-terraces. {100}-surfaces were found to be detrimental to high catalyst performance. The authors suggest that future catalyst design should either focus on procedures that contain poisons to deactivate {100}-surfaces or maximise {111}-terrace development.

Development and Application of 3D-PTV Measurements to Lab-Scale Stirred Vessel Flows

M. G. Romano, F. Alberini, L. Liu, M. J. H. Simmons and E. H. Stitt, *Chem. Eng. Res. Des.*, 2021, **172**, 71

3D particle tracking velocimetry (3D-PTV) was used to measure the flow of water in a laboratory-scale cylindrical tank at *Re* = 12,000, stirred using a six blade Rushton turbine. Different tracer concentrations and camera frame rates were investigated and optimised. The Savitzky–Golay filter was employed and optimised to enhance

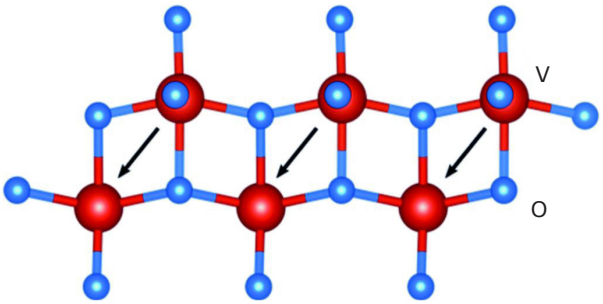

Fig. 1. Schematic illustration of polaron hopping direction in a V_2O_5 type phase. Reproduced from R. L. Gibson *et al.*, *Chem. Eng. Technol.*, 2022, **45**, (2), 238, with permission from the Royal Society of Chemistry

the signal-to-noise ratio of the measurements. Once the optimal conditions and filter were in place, the uncertainty in the tracer 3D positions was ~255 μm. An unbiased distribution of the flow timescales was ascertained from the autocorrelation of the Lagrangian velocity data. The method described could be used to assess the macro-mixing performance in various flow systems.

Electrochemical Enhancement of Reactively Sputtered Rhodium, Ruthenium, and Iridium Oxide Thin Films for Neural Modulation, Sensing, and Recording Applications

G. Taylor, R. Paladines, A. Marti, D. Jacobs, S. Tint, A. Fones, H. Hamilton, L. Yu, S. Amini and J. Hettinger, *Electrochim. Acta*, 2021, **394**, 139118

Pulsed-DC reactive magnetron sputtering was used to synthesise iridium oxide, ruthenium oxide and rhodium oxide thin films and the properties of these films were investigated. All oxide systems demonstrated that with increased working pressure, cathodic charge storage capacity increased and impedance decreased. This was measured using CV and electrochemical impedance spectroscopy (EIS). The improved electrochemical performance was attributed to the morphological changes that occurred alongside increased working pressure. The authors highlight that ruthenium oxide and rhodium oxide could be used as electrode coatings for neural interfacing devices. The electrochemical properties of iridium oxide were also reviewed.

Nuclear Spin Relaxation as a Probe of Zeolite Acidity: A Combined NMR and TPD Investigation of Pyridine in HZSM-5

N. Robinson, P. Bräuer, A. P. E. York and C. D'Agostino, *Phys. Chem. Chem. Phys.*, 2021, **23**, (33), 17752

2D ^{1}H NMR relaxation time measurements were used to investigate the relative surface affinities of pyridine within microporous HZSM-5 zeolites. As the silica to alumina ratio (SAR) decreased, an increase was observed in the pyridine surface affinity. This observation was verified by temperature-programmed desorption (TPD) analysis, which showed an increase in the heat of desorption linked to adsorbed pyridine as a function of diminishing SAR. The agreement between the TPD and NMR data suggested that NMR relaxation time analysis could be employed as a tool for the non-invasive characterisation of adsorption phenomena in microporous solids.

3D-PTV Flow Measurements of Newtonian and Non-Newtonian Fluid Blending in a Batch Reactor in the Transitional Regime

M. G. Romano, F. Alberini, L. Liu, M. J. H. Simmons and E. H. Stitt, *Chem. Eng. Sci.*, 2021, **246**, 116969

3D-PTV measurements were used to investigate the flow of non-Newtonian and Newtonian fluids in a laboratory-scale stirred vessel. The transitional flow regime was implemented and time-resolved tracer coordinates were used to calculate the Lagrangian accelerations and velocities in the flows. The Newtonian fluids had a higher impeller flow number than the non-Newtonian fluids. The Lagrangian velocity data was interpolated in a 3D Eulerian grid to generate the shear rate distributions. Initial investigation showed that the mean shear rate was proportional to the impeller rotational speed in the impeller region. However, further analysis demonstrated that Reynolds number and rheology also had influence.

An EPR Investigation of Defect Structure and Electron Transfer Mechanism in Mixed-Conductive $LiBO_2$-V_2O_5 Glasses

J. N. Spencer, A. Folli, H. Ren and D. M. Murphy, *J. Mater. Chem. A*, 2021, **9**, (31), 16917

A series of $LiBO_2$–V_2O_5 mixed conductive glasses, with varying V_2O_5 content, were studied using continuous wave EPR. A distinct exchange-narrowed signal was observed at high V_2O_5 content, while an isolated S = ½ vanadium defect centre was identified at a network modifying position at low V_2O_5. Modelling was used to examine the g-tensor and linewidth component of the EPR signals. Temperature dependent behaviour was observed, consistent with a polaron hopping mechanism of electron transfer and inter-electronic exchange along the g_3 direction (**Figure 1**). The activation energy was in line with other conducting glasses. Multi-frequency EPR measurements demonstrated that unaccounted for anisotropic exchange/speciation within the disordered network led to unresolved features at high frequencies.

$CuInS_2$ Quantum Dot and Polydimethylsiloxane Nanocomposites for All-Optical Ultrasound and Photoacoustic Imaging

S. Bodian, R. J. Colchester, T. J. Macdonald, F. Ambroz, M. Briceno de Gutierrez, S. J. Mathews, Y. M. M. Fong, E. Maneas, K. A. Welsby, R. J. Gordon, P. Collier, E. Z. Zhang, P. C. Beard, I. P. Parkin, A. E. Desjardins and S. Noimark, *Adv. Mater. Interfaces*, 2021, **8**, (20), 2100518

Quantum dot nanocomposites containing $CuInS_2$ quantum dots and medical-grade polydimethylsiloxane (CIS-PDMS) were engineered and applied to the distal ends of miniature optical fibres. The CIS-PDMS films demonstrated low optical absorption at near-infrared wavelengths greater than 700 nm and high optical absorption at 532 nm for ultrasound generation. The films generated ultrasound under pulsed laser irradiation. The coated optical fibre was paired with

a Fabry–Pérot fibre optic sensor to produce an ultrasound transducer, and the film was exploited to facilitate co-registered photoacoustic imaging and all-optical ultrasound of an ink-filled tube phantom.

Determining the Electrochemical Transport Parameters of Sodium-Ions in Hard Carbon Composite Electrodes

D. Ledwoch, L. Komsiyska, E.-M. Hammer, K. Smith, P. R. Shearing, D. J. L. Brett and E. Kendrick, *Electrochim. Acta*, 2022, **401**, 139481

Electrochemical potential spectroscopy (EPS), galvanostatic intermittent titration technique (GITT) and EIS were used to investigate the diffusivity and resistivity of sodium transport in hard carbon composite electrodes and various states-of-health. Impedance measurements and the diffusion coefficient from EPS and GITTS were used to extrapolate the charge transfer resistance, resistance contributions from the surface electrolyte interface and electrolyte transport in the electrode pores. The observed trends in desodiation, ageing and the diffusion coefficient during sodiation were similar for the different techniques. However, the orders of magnitude varied in the data. The calculated parameters were explored, and their accuracy examined.

Step Up: Gas–Liquid Mass-Transfer Characterization at Plant Scale Using the Pressure Step Method

R. W. Gallen, S. Smith, A. Burke and H. Stitt, *Ind. Eng. Chem. Res.*, 2021, **60**, (46), 16805

By accounting for background pressure loss, the authors adapted the pressure step method for use in a 1.3 m^3 vessel. The adapted method produced theoretically comprehensive results at rapid speeds. Hydrogen solubility in water was measured and the results were in agreement with the scientific literature. The overall mass-transfer coefficient was also measured. The measured values were compared to previously published modelling tools and correlations, which in turn demonstrated their poor predictive performance.

A Simple Liquid State ^{1}H NMR Measurement to Directly Determine the Surface Hydroxyl Density of Porous Silica

C. Penrose, P. Steiner, L. F. Gladden, A. J. Sederman, A. P. E. York, M. Bentley and M. D. Mantle, *Chem. Commun.*, 2021, **57**, (95), 12804

The authors present a quick and simple liquid ^{1}H NMR method to determine the surface hydroxyl density (a_{OH}) of silica with the use of a benchtop ^{1}H NMR spectrometer. The a_{OH} of fully hydroxylated silicas ranged from 4.16 OH nm^{-2} to 6.56 OH nm^{-2}, which aligned with previous studies in the literature. The cost, ease of use and speed associated with this method gives it an advantage over other techniques.

Selection of Formal Baseline Correction Methods in Thermal Analysis

R. L. Gibson, M. J. H. Simmons, E. H. Stitt, L. Horsburgh and R. W. Gallen, *Chem. Eng. Technol.*, 2022, **45**, (2), 238

An *in silico* study demonstrated the importance of choosing a suitable baseline correction method for thermal analysis data. Choosing the incorrect baseline correction led to a significant impact on the parameters obtained from kinetic modelling. A mass spectrometry dataset was employed to show the four formal baseline correction methods: linear with temperature, linear with time, no baseline correction and linear with extent of reaction. The authors recommended that Akaike weights should be compared to aid the selection of a correction method.